DOI:10.34918/87335

Maria ZADOŃ[1,*], Marek JASIŃSKI[1]

Chapter 9. NUMERICAL ANALYSIS OF THE EFFECT OF TEMPERATURE ON THE PARTIAL PRESSURE OF OXYGEN IN BIOLOGICAL TISSUE

9.1. Introduction

It can be said that all kinds of life activities in living organisms are related to the presence of oxygen. Oxygen is obtained in the lungs and then transported through the circulatory system to tissues from blood in the capillaries. The oxygen content in individual tissues is not constant and may vary depending on many factors, such as the degree of activity of the body, the external conditions in which the body is located, or the presence of various substances. Oxygen deficiency is known as hypoxia [1, 2].

An increase in the temperature of biological tissue can result from a variety of causes, such as physical exertion, medical conditions, or an external heat impulse. The latter factor often leads to changes in the thermophysical parameters of the tissue and even irreversible thermal damage to the tissue. Since thermal damage is associated with damage to the blood vessel network, among other things, it can ultimately affect oxygen delivery to the tissue. An increase in temperature also causes the so-called Bohr effect of shifting to the right the oxyhemoglobin dissociation curve, a sigmoidal function, which describes the relationship between the oxygenation of hemoglobin and the partial pressure of oxygen in the blood. The oxygen dissociation curve is laboratory--determine for specific values of temperature, carbon dioxide, pH, 2,3-DPG (2,3 diphosphoglycerate), and other substances [3–7].

[1] Department of Computational Mechanics and Engineering, Silesian University of Technology, Gliwice, Poland.
[*] Corresponding author: maria.zadon@polsl.pl.

9.2. The effect of temperature on oxygen transport in tissue

The relationship between saturation S_{Hb}, that is, the content of oxygen in the blood (more precisely in oxyhemoglobin), and the partial pressure of oxygen in the blood P_b is described by the sigmoidal oxyhemoglobin dissociation curve (ODC) (Fig. 1). The parameter that characterizes the dissociation curve is the P_{50} pressure corresponding to 50% hemoglobin saturation. An increase in temperature causes the P_{50} value to shift to the right, which is called the right shift effect or Bohr effect [1, 6, 7]. The ODC is described by various models, among which the Hill model is the most popular [1–3].

$$S_{Hb}(P_b) = \frac{P_b^n}{P_b^n + P_{50}^n} \tag{1}$$

where n denotes the Hill coefficient that is related to the slope of the dissociation curve. For normothermia, usually $P_{50} = 26$ [mmHg] and $n = 2.7$ are assumed [1–2]. Exemplary data for these parameters, depending on temperature, are presented in Table 1. The popularity of Hill's model is mainly due to the simplicity of the model and the ease of obtaining the inverse relationship necessary for computation of the oxygen distribution model:

$$P_b(S_{Hb}) = P_{50}\left(\frac{S_{Hb}}{1 - S_{Hb}}\right)^{\frac{1}{n}} \tag{2}$$

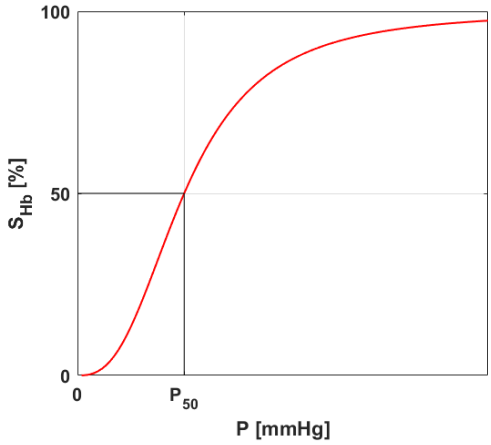

Fig. 1. Oxyhemoglobin dissociation curve
Rys. 1. Krzywa dysocjacji oksyhemoglobiny

Table 1

Temperature-dependent parameters of Hill model [6]

T [°C]	23	30	37	44
P_{50} [mmHg]	12.3	17.3	27.0	35.9
n	2.39	2.35	2.57	2.45

Tissue subjected to an external heat impulse can undergo thermal damage. The basic model for determining the degree of thermal damage to tissue is the Arrhenius scheme [8–10]:

$$Arr(\mathbf{x},t^F)=\int_0^{t^F} A\exp\left[-\frac{E}{RT(\mathbf{x},t)}\right]\mathrm{d}t \tag{3}$$

where T [K] is the temperature, R [J mol^{-1} K^{-1}] is the universal gas constant, E [J mol^{-1}] is the activation energy and A [s^{-1}] is the preexponential factor. The integral values of $Arr = 1$ and $Arr = 4.6$ correspond to a probability of 63% and 99% of cell death at a specific point **x**. Both values are used as criteria for tissue necrosis.

It is obvious that tissue damage can injure the blood vessel network within it. And because the presence of blood in biological tissue is described by the perfusion coefficient, a function can be created that maps the phenomena that occur in the tissue during the increase in temperature (the initial increase in perfusion during vasodilation) and subsequent thermal damage (the decrease in perfusion resulting from rupture of the vasculature [3, 8, 11]:

$$w(Arr)=\begin{cases}\left(1+25Arr-260Arr^2\right)w_0, & 0\le Arr\le 0.1\\ \left(1-Arr\right)w_0, & 0.1<Arr\le 1\\ 0, & Arr>1\end{cases} \tag{4}$$

where $w(Arr)$ and w_0 denote damage-dependent and initial perfusion coefficients [s^{-1}], respectively.

Changing tissue perfusion affects parameters associated with the oxygen distribution model, e.g., blood flow rate [cm^3 s^{-1}] and blood velocity [cm s^{-1}] [12].

9.3. Govering equations

In Figure 2 the models considered in the current work are presented. On the left, the considered domain of 3D biological tissue for thermal analysis is presented. The tissue

domain is exposed to the external heat impulse at the upper Γ_0 boundary. On the right, the Krogh cylinder-based model is visible to consider oxygen transport in tissue.

As mentioned previously, in the bioheat transfer model, the presence of blood is described by a perfusion coefficient. In practice, it is determined, among other things, by knowing the number of capillaries in the cross section or the volume of the tissue (depending on the method adopted). Thus, it is also possible to determine the velocity of blood in the capillary u_b based on knowledge of the perfusion coefficient and dimensions of the capillary [4]:

$$w = \frac{Q_b}{\pi R_t^2 L_t} = \frac{\pi R_c^2 u_b}{\pi R_t^2 L_t} \quad \rightarrow \quad u_b = w(Arr) L_t \frac{R_t^2}{R_c^2} \tag{5}$$

where Q_b [cm^3 s^{-1}] is the blood flow rate in the capillary, R_c, R_t, and L_t are the radius of the capillary radius, the tissue cylinder and length of cylinder, respectively.

This relationship was used to combine the bioheat transfer model and the oxygen distribution model. In the bioheat transfer model, points A-C have been highlighted, for which the curses of the determined parameters, including the perfusion coefficient, will be presented. For selected time steps, calculations will be carried out using the oxygen distribution model.

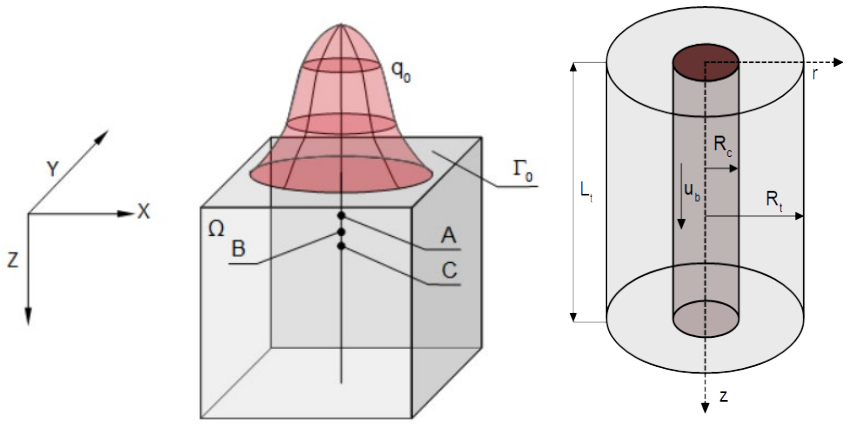

Fig. 2. Domains considered for the bioheat transfer and oxygen distribution model
Rys. 2. Obszary uwzględnione w modelu przepływu biociepła i dystrybucji tlenu

Bioheat transfer in the tissue domain Ω is described by the Pennes equation supplemented with appropriate boundary and initial conditions [8, 10, 11, 13]:

$$\begin{aligned}
&\mathbf{x} \in \Omega: \quad c\dot{T} = \nabla\left(\lambda \nabla T\right) + Q_{perf} + Q_{met} \\
&\mathbf{x} \in \Gamma_0: \quad q = q_0, \quad \text{for } t \le t_{exp}, \quad q = 0, \quad \text{for } t > t_{exp} \\
&\mathbf{x} \in \Gamma_c: \quad q = 0 \\
&t = 0: \quad T = T_{init}
\end{aligned} \tag{6}$$

where λ [W m^{-1} K^{-1}] is the thermal conductivity, c [J m^{-3} K^{-1}] is the volumetric specific heat of tissue and blood, Q_{met} [W m^{-3}] is the metabolic heat source, q_0 [W m^{-2}] is the boundary heat flux, t_{exp} [s] is the exposure time while T_{init} denotes the initial distribution of temperature, and the function of internal heat sources associated with perfusion Q_{perf} is as follows [8, 10]:

$$Q_{perf}(\boldsymbol{x}, t) = c_B w[T_B - T(\boldsymbol{x}, t)] \tag{7}$$

where c_B [J m^{-3} K^{-1}] is the volumetric specific heat of the blood, T_B corresponds to the temperature of the arterial blood.

Other thermophysical parameters of the tissue may also change as a result of an increase in its temperature. In the current work, the thermal conductivity λ is assumed to be temperature-dependent (temperature in Kelvin), whereas the volumetric specific heat c is treated as dependent on the thermal conductivity [10, 14]:

$$\lambda(T) = 0.6489 + 0.0427\, arctan[0.0252(T - 315.314)] \tag{8}$$

$$c(\lambda) = (3.385\lambda + 2.17) \cdot 10^6 \tag{9}$$

Separate equations for the radial and axial directions are applied for the Krogh cylinder model (cf. Fig. 2). For radial direction [2-4, 8, 12, 15]:

$$\begin{aligned} r \in \Omega_t: \quad & K_t \frac{1}{r}\frac{d}{dr}\left(r\frac{dP_t}{dr}\right) = M_t(P_t), \quad M_t(P_t) = \frac{M_0 P_t}{P_{crit} + P_t} \\ r = R_c: \quad & 2\pi R_c K_t \frac{dP_t}{dr} = -k\left(P_b - P_t\right) \\ r = R_t: \quad & \frac{dP_t}{dr} = 0 \end{aligned} \tag{10}$$

where P_t [mmHg] is the partial oxygen pressure in tissue, K_t [(cm^2 s^{-1})(mol cm^{-3} mmHg^{-1})] is the Krogh diffusion coefficient, M_0 [mol cm^{-3} s^{-1}] is the oxygen demand, P_{crit} [mmHg] is the partial pressure that corresponds to half maximum oxygen consumption, k [(cm^2 s^{-1}) (mol cm^{-3} mmHg^{-1})] is the mass transfer coefficient. The component $M_t(P_t)$ is the oxygen consumption in the tissue, assumed as the Michaelis-Menten kinetics.

Along the Krogh cylinder, the partial pressure of oxygen in the capillary P_b changes, which is expressed by the following relation [8, 12]:

$$\begin{aligned} z \in \Omega_c: \quad & Q_b \kappa_b \frac{d\left[S_{Hb}(P_b)\right]}{dz} = -k\left(P_b - P_t\right) \\ z = 0: \quad & P_b = P_{b\ inlet} \end{aligned} \tag{11}$$

where κ_b [mol cm$^{-3}_{blood}$] is the oxygen carrying a capacity of blood at 100% saturation, while S_{Hb} is the saturation of oxyhemoglobin, determined by the adopted model of oxyhemoglobin dissociation curve (2).

9.4. Methods of solution

In the stage of numerical implementation, an explicit scheme of the finite difference method was used to solve the bioheat transfer problem and shooting method to solve the oxygen distribution tasks.

The finite difference method uses the 7-point stencil shown in Fig. 3, with corresponding definitions of differential quotients (h is the grid step) [16]

$$\begin{aligned}
\left(\lambda\frac{\partial T}{\partial x}\right)^{f-1}_{i+0.5,j,k} &= \lambda_{01}\frac{T_1^{f-1}-T_0^{f-1}}{h} \quad \left(\lambda\frac{\partial T}{\partial x}\right)^{f-1}_{i-0.5,j,k} = \lambda_{02}\frac{T_0^{f-1}-T_2^{f-1}}{h} \\
\left(\lambda\frac{\partial T}{\partial y}\right)^{f-1}_{i,j+0.5,k} &= \lambda_{03}\frac{T_3^{f-1}-T_0^{f-1}}{h} \quad \left(\lambda\frac{\partial T}{\partial y}\right)^{f-1}_{i,j-0.5,k} = \lambda_{04}\frac{T_0^{f-1}-T_4^{f-1}}{h} \\
\left(\lambda\frac{\partial T}{\partial z}\right)^{f-1}_{i,j,k+0.5} &= \lambda_{05}\frac{T_5^{f-1}-T_0^{f-1}}{h} \quad \left(\lambda\frac{\partial T}{\partial z}\right)^{f-1}_{i,j,k-0.5} = \lambda_{06}\frac{T_0^{f-1}-T_6^{f-1}}{h}
\end{aligned} \tag{12}$$

where

$$\lambda_{0e} = \frac{2\lambda_0\lambda_e}{\lambda_0+\lambda_e}, \quad i = 1,\ldots,6 \tag{13}$$

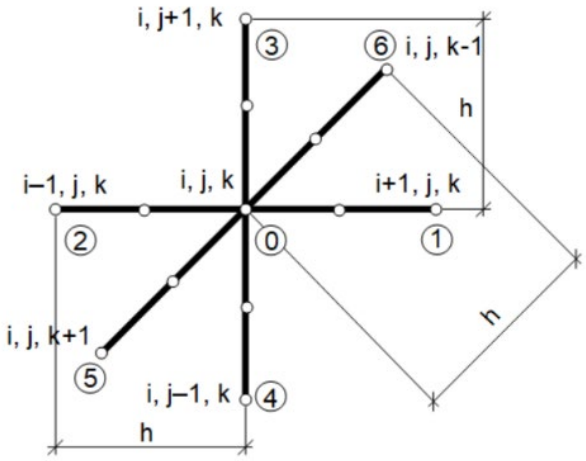

Fig. 3. 7-point stencil used in bioheat transfer problem
Rys. 3. 7-punktowa gwiazda stosowana w problemie przepływu biociepła

The idea of a shooting method is the transformation of a boundary value problem into an initial value problem (IVP). The boundary condition at the selected boundary of the domain under consideration is then used as the initial condition, while the second initial condition must be guessed. When the task is in this way, it can then be solved using one of the numerical methods for solving ODEs. The obtained value of the solution "on the second boundary" of the domain must be compared with the given boundary condition there. If the accuracy between the value of the one boundary condition and the obtained from IVP is not satisfactory, the initial value is guessed again and the problem is solved again [17, 18].

In the current work, the calculations of the shooting method were carried out in a Matlab 2022b environment. The secant method was used to determine the guess value and the fourth-order Runge-Kutta method for solving ODE [17].

9.5. Results of computations

In this work, a cube-shaped tissue domain with dimensions of 1.5 × 1.5 × 1.5 cm was considered. To reduce computational complexity, only a quarter of the area was taken into account. For the FDM analysis, the domain was discretized using 76 × 76 × 151 nodes. In the temperature determination, the Arrhenius injury integral and the perfusion coefficient the following data were used: c_B = 3.9962 [MJ m^{-3} K^{-1}], w_0 = [0.041 s^{-1}], Q_{met} = 245 [W m^{-3}], T_B = 37°C, q_0 = 15000 [W m^{-2}], t_{exp} = 30 [s], T_{init} = 37°C, A = 3.1e+98 [s^{-1}], E = 6.27e+5 [J mol^{-1}], R = 8.314 [J mol^{-1} K^{-1}] [3, 19, 20].

The calculations for the oxygen distribution model were carried out for the following data: R_c = 2.5 [μm], R_t = 25 [μm], L_t = 500 [μm], K_t = 4.1964e-14 [(cm^2 s^{-1})(mol cm^{-3} mmHg^{-1})], M_0 = 2.9762e-7 [mol cm^{-3} s^{-1}], P_{crit} = 1 [mmHg], k = 2.7902e-13 [(cm^2 s^{-1}) (mol cm^{-3} mmHg^{-1})], $P_{b\ inlet}$ = 100 [mmHg], κ_b = 8.9286e-6 [cm$^{-3}{}_{blood}$], n = 2.57, P_{50} = 27 [mmHg] [3, 12]. Based on the data contained in Table 1, the following functions were assumed to describe the parameters of the oxyhemoglobin dissociation curve P_{50} and n:

$$P_{50}(T) = \begin{cases} 27, & T < 37°\text{C} \\ 1.27T - 19.99, & T \in [37°\text{C}, 44°\text{C}] \\ 35.9, & T > 44°\text{C} \end{cases} \tag{14}$$

and

$$n(T)=\begin{cases}2.57, & T<37^{\circ}\mathrm{C}\\ -0.017T+3.199, & T\in[37^{\circ}\mathrm{C},44^{\circ}\mathrm{C}]\\ 2.45, & T>44^{\circ}\mathrm{C}\end{cases} \tag{15}$$

In the first step, the task related to determining the temperature distribution, tissue damage, and damage-dependent perfusion coefficient was solved. Then the values determined in this task for the selected node were used to solve tasks related to oxygen distribution.

Figure 4 shows distribution of temperature in the domain considered for 30 s and history of temperature at selected nodes, while Figure 5 presents distribution of the Arrhenius integral and perfusion coefficients for 10, 30 and 40 s. It can be seen that the Arrhenius integral exceeds both values of the necrosis criteria, i.e., $Arr > 1$ and $Arr > 4.6$. For the perfusion coefficient, both the areas of increased perfusion, above $w_0 = 0.041$ [s^{-1}], and the area where, due to exceeding $Arr > 1$, the perfusion disappeared (cf. equation (4)) are clearly visible. Figure 6 is also related to the bioheat transfer analysis and presents history of the Arrhenius integral and the perfusion coefficient at the selected nodes.

For the analysis of oxygen distribution, point B (cf. Fig. 2) was selected.

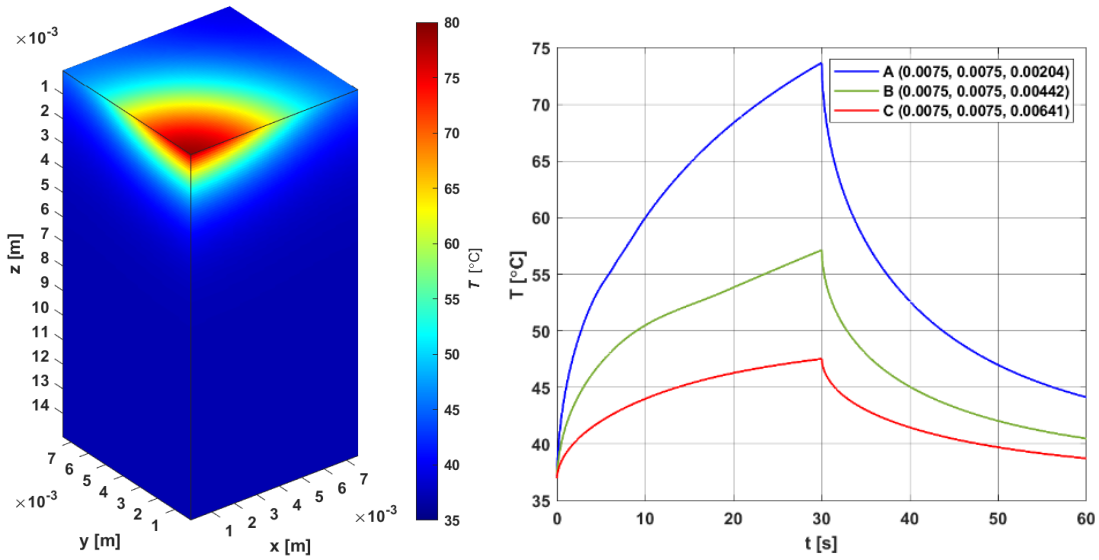

Fig. 4. Distribution of temperature for 30 s and history of temperature at selected nodes
Rys. 4. Rozkład temperatury dla 30 s oraz historia temperatury w wybranych węzłach

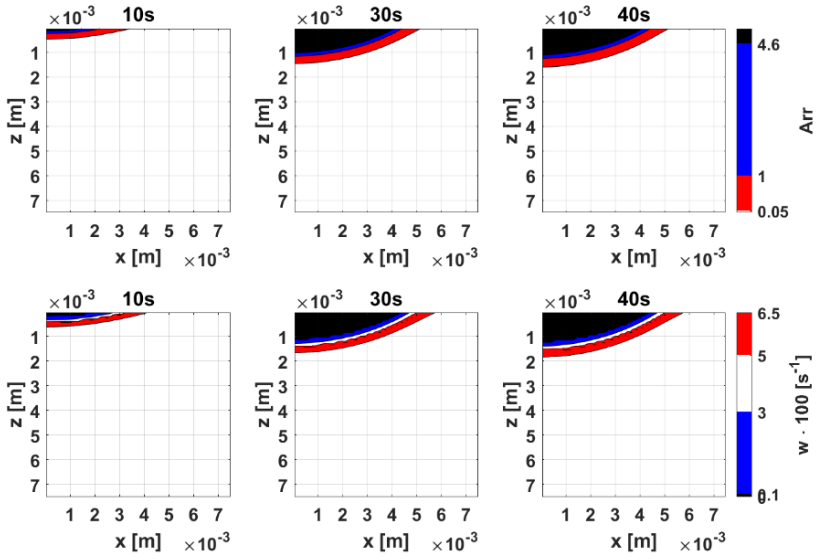

Fig. 5. Distribution of the Arrhenius integral and perfusion coefficient for 10, 30 and 40 s
Rys. 5. Rozkład całki Arrheniusa i współczynnika perfuzji dla 10, 30 i 40 s

Based on the history of the perfusion coefficient and equation (5) the blood velocity in the capillary u_b was calculated for selected time steps: 0, 10,…, 60 s. The following variants of simulation were conducted:

– variant 1: constant u_b, variable P_{50} and n,
– variant 2: variable u_b, constant P_{50} and n,
– variant 3: variable u_b, variable P_{50} and n.

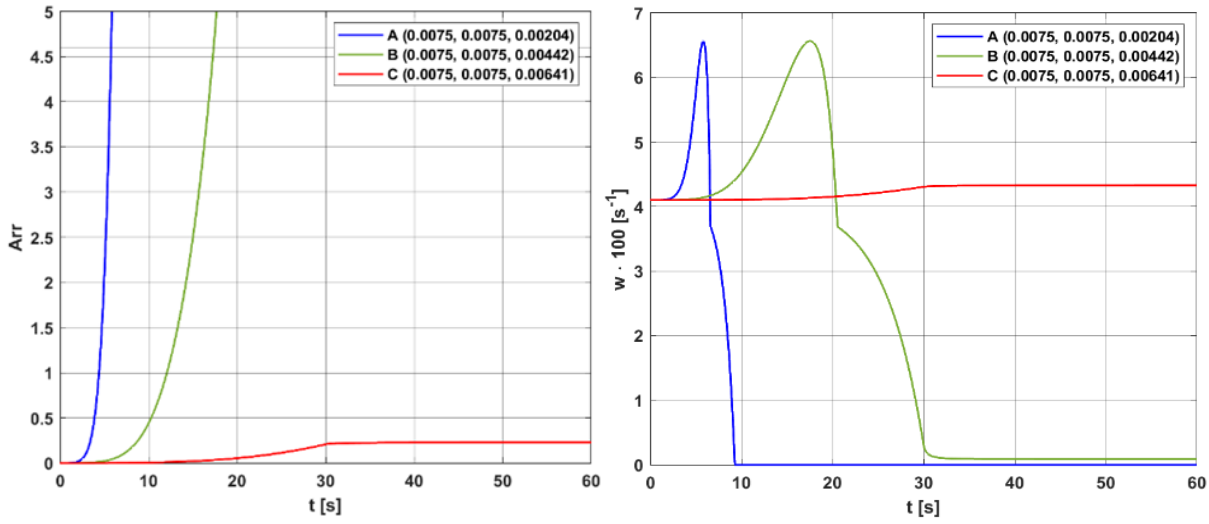

Fig. 6. History of Arrhenius integral and perfusion coefficient at selected nodes
Rys. 6. Historia całki Arrheniusa i współczynnika perfuzji w wybranych węzłach

The assumption of the constant parameter values means that their values for $t = 0$ are used (i.e. associated with T_{init} = 37°C, $w = w_0 = 0.041$ [s^{-1}]), while the variable parameters are related to u_b estimated on the basis of equation (5) and/or P_{50} and

n estimated on the basis of equations (14) and (15). The variant with constant u_b and constant Hill curve parameters was not considered because it corresponds to the simulations for $t = 0$, for each of the calculation variants. As is visible, the hypoxia phenomenon, that is, a drop in the partial pressure of oxygen in the capillary to zero before the end of the capillary, occurs only for variants 2 and 3.

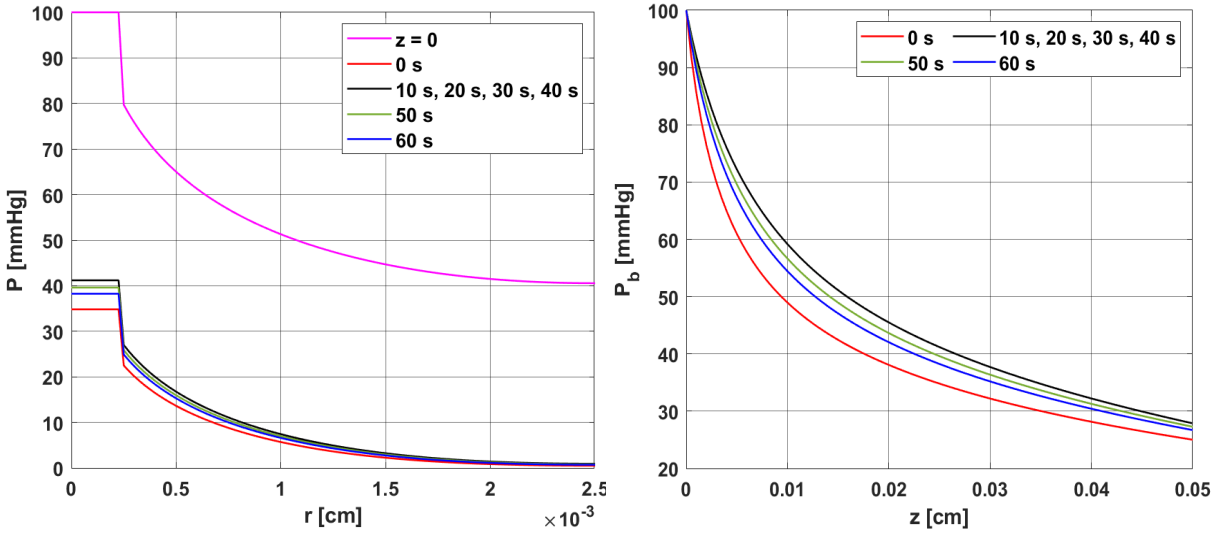

Fig. 7. Distribution of partial pressure in radial and axial directions in variant 1 (constant u_b, variable P_{50} and n)

Rys. 7. Rozkład ciśnienia parcjalnego w kierunku promieniowym i osiowym dla wariantu 1 (stałe u_b, zmienne P_{50} i n)

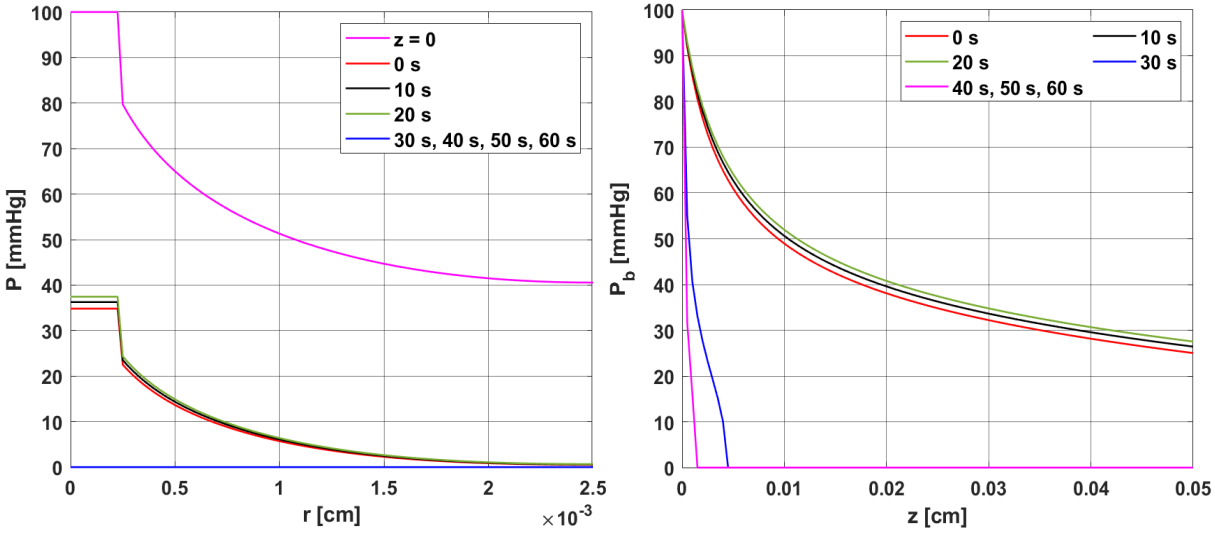

Fig. 8. Distribution of partial pressure in radial and axial directions in variant 2 (variable u_b, constant *P50* and n)

Rys. 8. Rozkład ciśnienia parcjalnego w kierunku promieniowym i osiowym dla wariantu 2 (zmienne u_b, stałe *P50* i n)

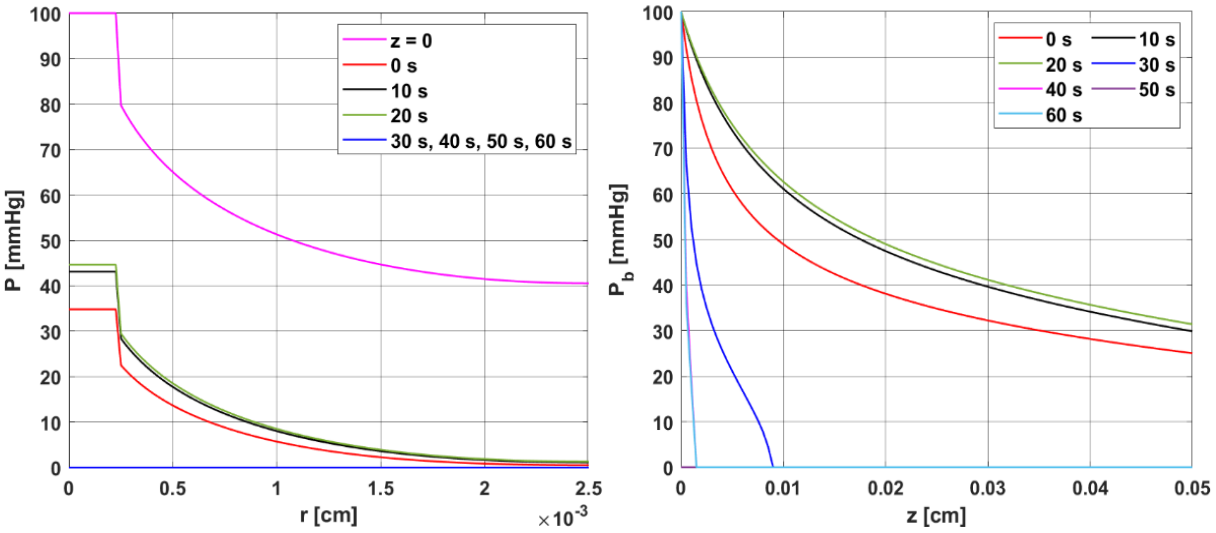

Fig. 9. Distribution of partial pressure in radial and axial directions in variant 3 (variable u_b, P_{50} and n)
Rys. 9. Rozkład ciśnienia parcjalnego w kierunku promieniowym i osiowym dla wariantu 3 (zmienne u_b, P_{50} i n)

9.6. Conclusions

The simulation cases show that the appearance of the hypoxia phenomenon was mainly influenced by the change in blood velocity resulting from the value of the perfusion coefficient value. The latter was closely related to thermal tissue damage through function (4). A drop in the perfusion value causes a simultaneous decrease in blood velocity. The effect of dependence of Hill curve parameters on temperature causes an increase in pressure with increasing temperature. In situations such as those of variant 3, it can counteract the occurrence of hypoxia.

It should be pointed out that many of the parameters used in the simulations were assumed to be constant values, e.g. $P_{b\,inlet}$. Thermal damage can cause changes at different levels of the vascular network, so this value should also be accepted as related to tissue damage. It is also worth noting that part of the function (4) is defined in connection with dilatation of the blood vessels ($0.1 < Arr \leq 1$), which in the model related to temperature distribution and determining the degree of tissue damage means an increase in perfusion, while in the oxygen distribution model it could mean a change in diameter of the capillary R_c.

The overall model presented shows that the phenomenon of thermal damage is complex, not limited to one type of phenomena. In addition, there are suggestions in the literature about the effect of oxygen on some kind of reversal of the thermal damage phenomenon, which may be important, especially when modeling various types of

therapies in which the temperatures used are not high. Attempts have been made to account for this phenomenon by attaching an additional component to the Arrhenius integral [9].

Bibliography

1. D. Goldman, Theoretical models of microvascular oxygen transport to tissue, *Microcirculation*, (2008) **15**(8): 795–811.
2. A.S. Popel, Theory of oxygen transport to tissue, *Critical Reviews in Biomedical Engineering*, (1989) **17**(3): 257–321.
3. M. Jasiński, Numerical analysis of the temperature impact to the oxygen distribution in the biological tissue, *Journal of Applied Mathematics and Computational Mechanics*, (2020) **19**(3): 17–28.
4. B.C. Fry, T.K. Roy, T.W. Secomb, Capillary recruitment in a theoretical model for blood flow regulation in heterogeneous microvessel networks, *Physiological Reports*, (2013) **1**(3): e00050.
5. T.W. Secomb, J.P. Alberding, R. Hsu, M.W. Dewhirst, A.R. Pries, Angiogenesis: An adaptive dynamic biological patterning problem, *PLoS Computational Biology*, (2013) **9**(3): e1002983.
6. M.P. Hlastala, R.D. Woodson, B. Wranne, Influence of temperature on hemoglobin-ligand interaction in whole blood, *Journal of Applied Physiology*, (1977) **43**(3): 545–550.
7. M. Castaing, M. Sinet, Temperature and oxygenation of human blood at constant total CO2 content, *Pflugers Archiv, European Journal of Physiology*, (1980) **386**(2): 135–140.
8. M. Jasiński, Numerical analysis of thermal damage and oxygen distribution in laser irradiated tissue, *Journal of Applied Mathematics and Computational Mechanics*, (2022) **21**(2): 51–62.
9. L.A. Dombrovsky, Laser-induced thermal treatment of superficial human tumors: An advanced heating strategy and non-Arrhenius law for living tissues, *Frontiers in Thermal Engineering*, (2022) **1**: 807083.
10. J.T. Oden, K.R. Diller, C. Bajaj, J.C. Browne, J. Hazle, I. Babuška, J. Bass, L. Biduat, L. Demkowicz, A. Elliott, Y. Feng, D. Fuentes, S. Prudhomme, M.N. Rylander, R.J. Stafford, Y. Zhang, Dynamic data-driven finite element models for laser treatment of cancer, *Numerical Methods for Partial Differential Equations*, (2007) **23**(4): 904–922.

11. J.P. Abraham, E.M. Sparrow, A thermal-ablation bioheat model including liquid-to-vapor phase change, pressure- and necrosis-dependent perfusion, and moisture-dependent properties, *International Journal of Heat and Mass Transfer*, (2007) **50**(13-14): 2537–2544.
12. B.J. McGuire, T.W. Secomb, A theoretical model for oxygen transport in skeletal muscle under conditions of high oxygen demand, *Journal of Applied Physiology*, (2001) **91**(5): 2255–2265.
13. B. Mochnacki, M. Ciesielski, Sensitivity of transient temperature field in domain of forearm insulated by protective clothing with respect to perturbations of external boundary heat flux, *Bulletin of the Polish Academy of Sciences: Technical Sciences*, (2016) **64**(3): 591–598.
14. G. Hamilton, Investigations of the thermal properties of human and animal tissues, Ph. D. Thesis, University of Glasgow, UK, (1998).
15. Y. He, M. Shirazaki, H. Liu, R. Himeno, Z. Sun, A numerical coupling model to analyze the blood flow, temperature, and oxygen transport in human breast tumor under laser irradiation, *Computers in Biology and Medicine*, (2006) **36**(12): 1336–1350.
16. E. Majchrzak, B. Mochnacki, Dual-phase lag equation. Stability conditions of a numerical algorithm based on the explicit scheme of the finite difference method, *Journal of Applied Mathematics and Computational Mechanics*, (2016) **15**(3): 89–96.
17. A.Ü. Keskin, Boundary Value Problems for Engineers, Springer International Publishing, Heidelberg, (2019).
18. B.S. Attili, M.I. Syam, Efficient shooting method for solving two point boundary value problems, *Chaos, Solitons & Fractals*, (2008) **35**(5): 895–903.
19. E. Majchrzak, L. Turchan, M. Jasiński, Identification of laser intensity assuring the destruction of target region of biological tissue using the gradient method and generalized dual-phase lag equation, *Iranian Journal of Science and Technology – Transactions of Mechanical Engineering*, (2019) **43**: 539–548.
20. M. Jasiński, M. Zadoń, Mathematical modeling of the phenomena that occur in a biological tissue containing a photosensitizer, *Journal of Applied Mathematics and Computational Mechanics*, (2023) **21**(4): 40–51.

NUMERICAL ANALYSIS OF THE EFFECT OF TEMPERATURE ON THE PARTIAL PRESSURE OF OXYGEN IN BIOLOGICAL TISSUE

Abstract

The impact of an external heat pulse causes an increase in the tissue's temperature, resulting in a change in the tissue's thermophysical parameters and even irreversible thermal damage to the tissue. Damage to the blood vessel system can also affect oxygen delivery to the tissue. An increase in temperature causes the so-called Bohr effect, which affects the oxyhemoglobin dissociation curve describing the relationship between the oxygenation of hemoglobin and the partial pressure of oxygen in the blood. The work concerns the numerical analysis of the process of heating biological tissue and its thermal damage under the influence of an external heat impulse. The analysis is based on the bioheat transport equation in Pennes form. Using the Arrhenius scheme, the degree of thermal damage to the tissue is estimated, and, tissue parameters are treated as temperature-or damage-dependent. A model based on the Krogh cylinder concept was used to analyze changes in oxygen distribution in the capillary vessel and surrounding tissue. A Hill model was used to describe the oxyhemoglobin dissociation curve. Variable values of the parameters of dissociation curve and the blood velocity in the capillary were considered. The oxygen distribution model is linked to the thermal model through the relationship between the blood velocity in the capillary and the perfusion coefficient. In the stage of numerical realization, the finite difference method and the shooting method were used.

Keywords: bioheat transfer, tissue thermal damage, oxygen transport, finite difference method, shooting method